Highlights

Metal doping of dielectric thin layers by electric field assisted film dissolution

Boris Okorn, Jordi Sancho-Parramon, Miodrag Oljaca, Vesna Janicki

- Dielectric thin film metal doping performed by electric field assisted dissolution.
- Numerical modelling reveals dopant ion distribution time evolution.
- Doping values and time-scale are correlated with material parameters.
- Doping evolution in Ag/SiO_2/glass can be optically tracked by ellipsometry.

Metal doping of dielectric thin layers by electric field assisted film dissolution

Boris Okorn[a], Jordi Sancho-Parramon[a], Miodrag Oljaca[b], Vesna Janicki[a,*]

[a]*Ruđer Bošković Institute, Bijenička cesta 54, 10000 Zagreb, Croatia*
[b]*Koura (part of Orbia), 950 Winter Street, Waltham MA 02451, USA*

Abstract

The incorporation of metal ions in dielectric layers by means of electric field assisted film dissolution is investigated. The samples consist of alkali-containing glass substrates coated first with SiO_2 and then Ag thin films. The application of moderately elevated temperatures and DC voltages induces thermal poling in the glass matrix and metal film dissolution, resulting in the incorporation of metal ions in both dielectric layer and glass matrix. First, the process dynamics are simulated by modelling the migration of metal film ions and alkali species under an applied electric field. Numerical solution of the model indicates that metal ions progressively dope the dielectric layer until they reach the glass matrix. Then the dopant distribution in the layer becomes steady-state and further injection of ions contributes to increase the dopant concentration in glass. The influence on the process of alkali and dopant ion mobilities and alkali ion concentration is analysed. Additionally, Ag doping of SiO_2 layers deposited on soda-lime and borosilicate glasses is experimentally carried out and characterized using spectroscopic ellipsometry. The evolution of refractive index profiles through both, SiO_2 layer and glass substrate, is correlated with ion migration and confirms the model trends. Overall, this study shows that glass poling

*Corresponding author. E-mail: janicki@irb.hr

and film dissolution can be used to control metal doping of dielectric layers, with potential application in optical and photonic devices.

Keywords: metal doping, glass poling, electric field assisted dissolution, refractive index, ellipsometry

---

1. Introduction

Glass matrix doped with metal ions has been a subject of interest for a long time due to its multiple application possibilities, including optical waveguides, antimicrobial substrates or formation of metal-dielectric nanocomposites with plasmonic properties [1]. A wide range of techniques have been developed for the fabrication of metal-doped glass, such as ion-implantation, sol-gel and ion-exchange, the last being the most widespread method due to its versatility [2]. In an ion-exchange process, glasses containing alkali ions are placed in a molten salt solution rich in metal ions. The ions from the solution penetrate in the glass and partially replace alkali ions that out-diffuse the glass matrix. The ion diffusion process can be additionally controlled by an external DC voltage [3].

It has been shown that metal films deposited on glass can be an efficient ion source for field assisted ion-exchange [4, 5, 6]. Electric field assisted dissolution (EFAD) of metal films has been also used to dissolve nanoparticles embedded in, or deposited on, thin dielectric layers [7, 8, 9, 10]. These works have essentially focused on metal film dissolution as a mechanism to largely modify the samples optical response by quenching the nanoparticles surface plasmon resonance or metal film absorption. Less attention has been devoted to the possible doping of dielectric thin films in these processes. We have recently observed that Ag ions resulting from EFAD appear to be located close to the film/glass interface rather than in the dielectric film [9]. Dielectic thin film metal doping by EFAD could have a strong application potential

for it would enable fine tuning of optical and electrical properties of films using a well-established methodology.

In this work we investigate how the EFAD process takes places in a metal/ dielectric/glass multilayer system. We first model the diffusion process taking into account drift and diffusion of glass alkali ions and externally injected metal dopant ions. The model simulations help in understanding the process dynamics and elucidates the role of different material properties. Additionally, we fabricated Ag/SiO_2/glass samples and induced EFAD of Ag film. In order to characterize this process, the evolution of the sample optical properties is tracked by spectroscopic ellipsometry, a technique able to accurately track modifications in glass surfaces by optical means [11, 12]. SIMS measurements confirm the trends suggested from ellipsometric data analysis. In summary, the experimental results verify the insights obtained by model simulations and indicate how to control the EFAD process for an efficient doping of dielectric thin films with metal ions.

2. Materials and Methods

All samples consist of a 1 mm thick glass substrate coated with a 500 nm thick SiO_2 layer and then with a 50 nm thick Ag over-layer. The films were deposited by electron beam evaporation using a modified Varian chamber. The glass substrate was either soda-lime (SL) or borosilicate (BK7) glass slides. The amount of deposited material was controlled using a quartz crystal monitor, the base pressure was 6×10^{-6} Torr and the deposition rate was ≈ 1 Å/s for Ag and ≈ 10 Å/s for SiO_2.

The fabricated samples were sandwiched between a flat Cr-coated glass anode and an Al cathode and placed in an oven (Lindberg Blue M ThermoScientific). The samples were pre-heated for 40 minutes at 200 °C. A DC voltage of 200 V was applied (Keithley 2290-5 power supply) for a time ranging between 5 minutes and

1 hour at the mentioned temperature. The samples were then allowed to cool down to room temperature. These treatment conditions lead to a partial EFAD of the Ag layer except for the SL sample treated for 1 hour, in which Ag appeared to be completely dissolved. The undissolved metal remains were mechanically removed from the sample surface.

Ellipsometric measurements of the treated samples were taken with a J. A. Woollam V-VASE ellipsometer in the range 0.57-4.5 eV at different angles of incidence (45°, 55° and 65°). The WVASE software was used to model the in-depth refractive index variations and fit ellipsometric data. Secondary ion mass spectrometry (SIMS) measurements were performed on selected samples to validate the conclusions from the ellipsometric data analysis.

3. Numerical simulations

Modelling the ion migration process in field assisted ion exchange processes requires taking into account drift and diffusion ionic currents and the resulting electric field spatial variations [13, 14]. The basic equations describing these mechanisms have been extended to model electrical currents in poling of silica glasses [15], sequential ion-exchange of several species [16] and external injection of hydrogen species [17, 18], even in presence of multiple alkali species in the glass matrix [19]. In this Section we adapt these modelling approaches to analyse the metal/dielectric/glass system.

3.1. Ion dynamics model

Let us consider a glass substrate of thickness W coated with a dielectric layer of thickness h. The sample is placed between two electrodes subjected to a DC voltage U and with the dielectric layer facing the anode. The sample depth is represented by the x coordinate with $x = 0$ taken at the glass/dielectric layer interface, $x > 0$

indicating the glass and $x < 0$ the dielectric layer (see Figure 1). We assume that the glass contains a single species of monovalent alkali ions (typically Na^+) with a position and time-dependent concentration given by $C_a(x,t)$. Dopant ions can be injected from the anode (metal film) and their concentration evolution is represented by $C_d(x,t)$. Defining the initial total ion concentration as $C_0(x) = C_a(x,0) + C_d(x,0)$, the evolution of the system is given by the following partial differential equations:

$$\frac{\partial C_a}{\partial t} = \mu_a \frac{\partial (EC_a)}{\partial x} + D_a \frac{\partial^2 C_a}{\partial x^2} \tag{1}$$

$$\frac{\partial C_d}{\partial t} = \mu_d \frac{\partial (EC_d)}{\partial x} + D_d \frac{\partial^2 C_d}{\partial x^2} \tag{2}$$

$$\frac{\partial E}{\partial x} = \frac{e}{\varepsilon_0 \varepsilon} (C_a + C_d - C_0) \tag{3}$$

where E is the local electric field, μ_a (μ_d) and D_a (D_d) are the alkali (dopant) ion mobility and self-diffusion coefficients, e is the electron charge, ε_0 the vacuum permittivity and ε the relative permittivity. The first two equations describe the time evolution of ions as a result of drift and diffusion currents while the last one is Poisson's equation. Appropriate initial and boundary conditions have to be set in order to solve this system of equations. The first boundary condition is given by the externally controlled applied DC potential:

$$\int_{-h}^{W} E dx = U \tag{4}$$

Additionally, the following conditions are related to the ion concentrations:

$$C_a(x \leq 0, 0) = 0 \tag{5}$$

$$C_a(x > 0, 0) = C_{a0} \tag{6}$$

$$C_d(x, 0) = 0 \tag{7}$$

$$\frac{\partial C_d(-h,t)}{\partial t} = \alpha E(-h,t) \tag{8}$$

The first three conditions state the initial concentration of alkali and dopant ions through the sample. The last condition enables dopant ion migration into the sample and establishes that the ion injection rate is proportional to the strength of the electric field at the anode, α being the proportionality constant [18]. The system of differential equations has been numerically solved using the Runge-Kutta algorithm [20].

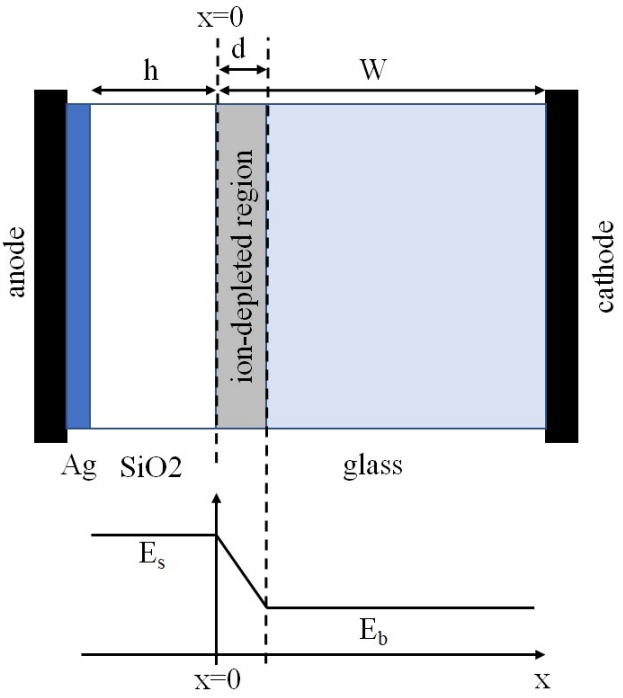

Figure 1: Scheme of the model used for simulations (top) and typical electric field distribution in conventional glass poling experiment, i.e. without external injection of ions (bottom).

3.2. Computational results

Simulations of the ion migration process are carried out in all cases setting $U =$ 1000 V, $T = 200$ °C and $\alpha = 3 \cdot 10^{16}$ $\mathrm{m^{-2}V^{-1}s^{-1}}$ in a sample with $W = 1$ mm, $h =$ 500 nm and $\varepsilon = 10$. It is difficult to determine a realistic value of α from literature

data but we have observed that the process dynamics is, from a qualitative point of view, weakly affected by this parameter. Although ion mobility can be significantly dependent on the local environment [21], for the sake of simplicity we consider that μ_a, μ_d and ε take the same value in the glass and in the dielectric layer. It is assumed that ion mobility and self-diffusion coefficients are connected through the Nernst-Einstein relation, $\mu_i = eD_i/kT$, k being Boltzmann's constant.

It is convenient first to recall the alkali ion migration dynamics in a standard thermal poling process [21]. Due to the applied voltage and temperature-enhanced mobility, ions drift away from the anode leaving place to an ion-depleted region where the electric field linearly decays from the anode (E_s) to the beginning of the non-depleted zone (E_b) [22]. The thickness and electric field in the ion-depleted region increase with time, approaching to an steady-state in which most of the applied potential falls at the depletion region and E_b tends to zero. The characteristic time constant (τ) of this process is given by $Wd/\mu_a U$ where d is the steady-state value of the ion-depleted region ($d = \sqrt{2\varepsilon_0\varepsilon U/eC_{a0}}$). If a pure dielectric layer is present on top of the glass side that faces the anode (Figure 1), according to Poisson's equation the electric field within the layer remains constant and equal to E_s, for no ions leave or enter the layer.

Let us now consider the model described in the previous subsection. Figure 2 illustrates the ion migration in a system with $\mu_a = 10^{-16}$ $\mathrm{m^2V^{-1}s^{-1}}$, $\mu_d = 10^{-15}$ $\mathrm{m^2V^{-1}s^{-1}}$ and $C_{a0} = 10^{27}$ $\mathrm{m^{-3}}$. Larger mobility of dopant ions in glass with respect to alkali ions has been reported in [23] and [24]. These parameters lead to values of $d \approx 33$ nm and $\tau \approx 330$ s. At the beginning of the process, the electric field grows in both, glass depletion region and dielectric layer, enabling the injection of dopant ions into the layer and their diffusion towards glass. The implantation depth advances with time at a growing rate because the electric field in the layer increases

while the depletion layer is still being formed. After some time ($\approx$ 2 s, as suggested from Figure 2) the dopant ions reach the glass matrix, where they move more slowly than in the layer due to the smaller electric field values. This speed difference leads to an accumulation of dopant ions at the glass region next to the layer. Note that C_d at the glass interface remains well below C_{a0} and that the injection of Ag does not compensate the depletion of alkali ions. On the other hand, the presence of ions in the originally neutral layer generates an electric field gradient ($\partial E/\partial x > 0$) that results in a progressive decrease of E_s. Eventually, the dopant ion distribution in the layer reaches steady-state because the anode-to-layer ion injection rate is constant ($E(-h,t) = 0$, as seen in the right panel of Figure 2, hence $\partial C_d(-h,t)/\partial t = 0$) and equal to the layer-to-glass matrix ion injection rate. This steady-state situation is clearly observed in Figure 3, that shows the amount of incorporated ions ($\int C_d dx$) in the layer and in the glass: once the ions reach the glass matrix, their distribution in the dielectric layer quickly stabilizes and further injection of ions increases the amount of dopant in the glass matrix only.

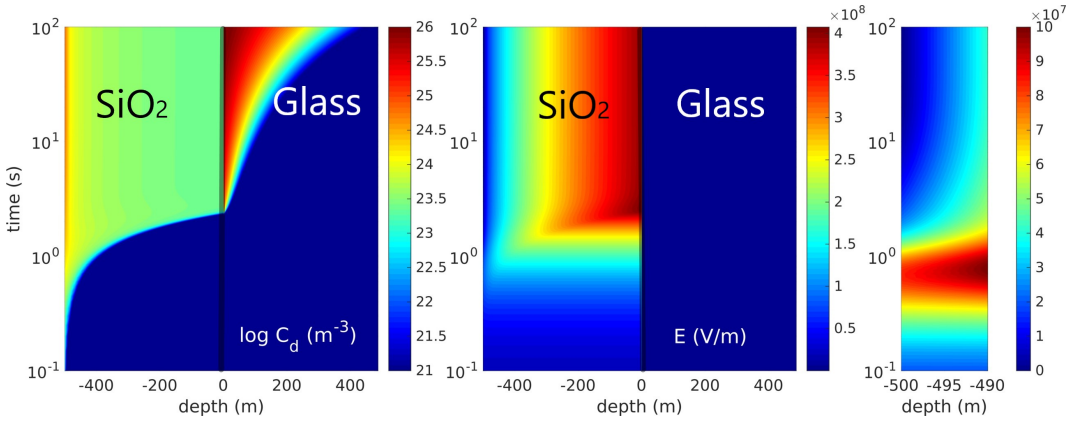

Figure 2: Time and depth evolution of dopant ion concentration (logarithmic scale, left) and electric field (center and right) for the case of μ_a =10^{-16} m^{2}V^{-1}s^{-1}, $\mu_d = 10^{-15}$ m^{2}V^{-1}s^{-1} and $C_{a0} = 10^{27}$ m^{-3}. Vertical lines indicate the glass/dielectric layer interface. The right panel shows an enlarged view of the electric field distibution in the region near the surface of the sample facing the anode.

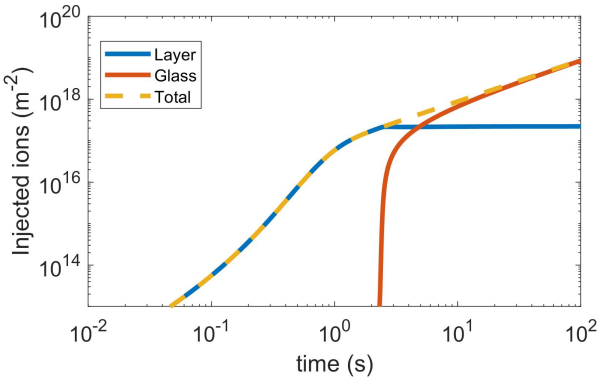

Figure 3: Time evolution of the total amount of ions injected in the glass, dielectric layer and its sum. Simulation parameters same as in Figure 2.

In order to analyse the role of glass and dopant ions properties in the process, several parameters were varied with respect to the previous simulation (Figure 4). The top panel shows the dopant distribution evolution when the alkali ion mobility is reduced by one order of magnitude (μ_a =10^{-17} $\mathrm{m^2V^{-1}s^{-1}}$), which increases τ by one order of magnitude while d is unchanged. Thus, the growth of the electric field in the dielectric layer is now slower and the dopant ions take longer to reach the glass and start to diffuse there. The middle panel shows the situation where alkali concentration is reduced by two orders of magnitude and again τ, but now also d, increase by one order of magnitude. Now the process also takes place more slowly, but the ion-depletion region is larger and the values of E_s are consequently smaller. Therefore, the dopant ions need longer time to reach the glass matrix and the accumulation of ions in the layer is much lower than in the previous case. Finally, the last panel shows the situation in which the dopant ions have one order of magnitude lower mobility. Now d and τ do not change but the dopant ions take longer to reach the glass surface. Thus E_s achieves larger values before the steady state is achieved, leading to a higher injection rate and more ions remaining in the layer.

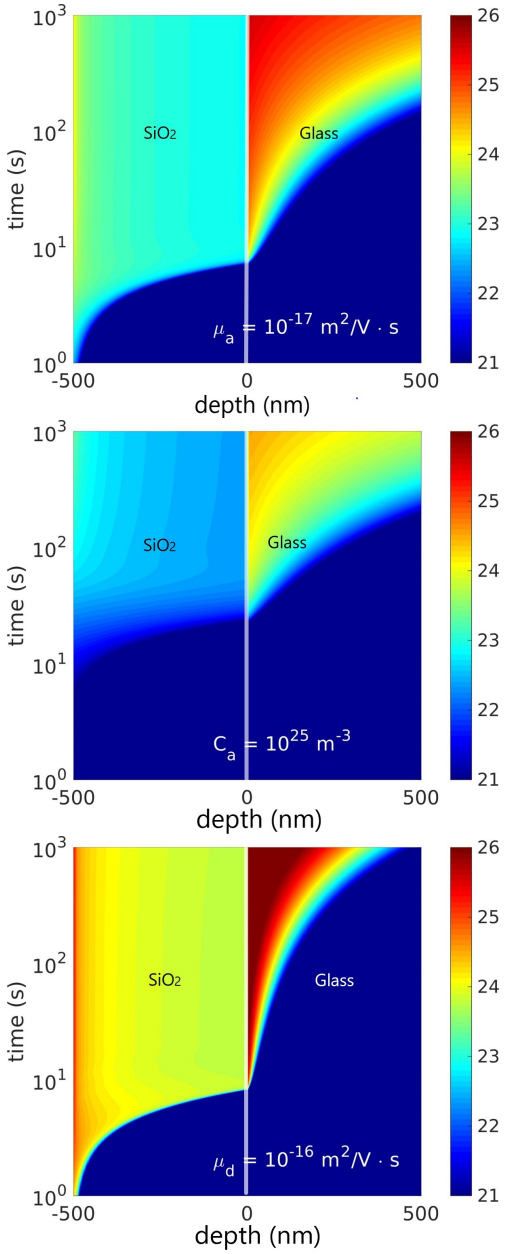

Figure 4: Time and depth evolution of dopant ion concentration (logarithmic scale) with one of the simulation parameters (μ_a - top, C_{a0} - middle, μ_d - bottom) having values smaller than those in the simulation of Figure 2. For the sake of comparison, the time scale is different with respect to the previous simulation but the concentration scale limits are the same. Vertical lines indicate the glass/dielectric layer interface.

4. Experimental results

As mentioned before, the applied EFAD conditions have resulted in incomplete film dissolution on the fabricated samples. Therefore, the Ag film can be treated as a permanent ion-source and the samples comply with the described model assumptions. Ellipsometric measurements are fitted by means of a three-layer model: 1) an unmodified glass substrate in bulk, with the optical constants of untreated glass, 2) a modified glass region where the refractive index is altered by the presence of dopant ions and depletion of alkali ions and 3) a top SiO_2 layer with refractive index modified by the dopant ions. The refractive indices of these two last layers are expected to show an in-depth variation according to the non-homogeneous dopant concentration profiles. Theoretical and experimental work on ion-exchange processes state a linear relation between Ag ion concentration and refractive index modification [25, 26, 27]. Taking into account that Ag doping has a moderate influence on the refractive index dispersion, [28], the depth and wavelength (λ) refractive index dependence is modelled with the following Cauchy expression:

$$n\left(x,\lambda\right)=n_0\left(x\right)+\frac{n_1}{\lambda^2}. \tag{9}$$

A polynomial variation of n_0 with the sample depth ($n_0\left(x\right)=a_0+a_1x+...+a_px^p$) was assumed for both SiO_2 and modified glass layers. The degree of the polynomial p was increased until no significant improvement of fitting quality was obtained, with p being 3 in most cases. This approach enables progressive extension of model complexity while keeping the number of optimized parameters at a minimum. Figure 5 illustrates the data fitting quality for a representative sample.

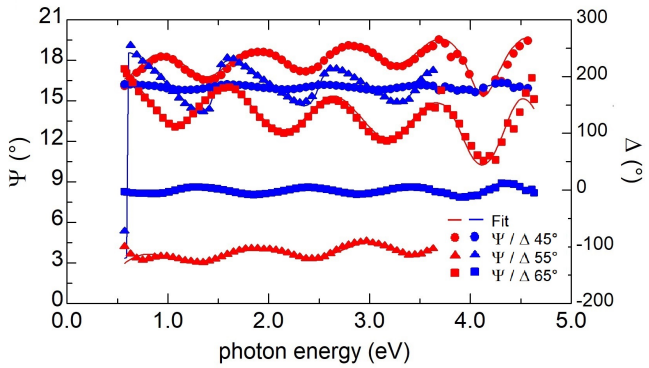

Figure 5: Ellipsometric functions (top: Δ, bottom: Ψ) at different angles of incidence for the SL sample treated for 40 min. Experimental measurements are represented by symbols and best fits by solid lines.

The obtained refractive index profiles are shown in Figure 6. In the case of SL samples, for treatment times up to 20 minutes the refractive index of the SiO_2 layer increases with time. The refractive index is larger than in pure dielectric layer produced for comparison ($n = 1.44$). The largest index variation is obtained in the region next to the layer side facing the anode. The refractive index is also increasing with time in the substrate region next to the dielectric layer. These refractive index trends are in accordance with those observed for the simulated dopant concentration profiles. Long treatment times result in a lowering of the refractive index in the substrate region next to the layer, that could be explained by the depletion of alkali ions as discussed below. However, the SiO_2 layer refractive index is also reduced beyond the values of pure layers, particularly in the region next to the substrate. We have verified that this change is not associated to a temperature-related modification of the SiO_2 layer, in agreement with previous results [29]. This effect points to a reduced material density that could result in a damaged layer. Indeed, recent works reported glass cracking in Ag ion exchanged soda-lime glass that has been associated to increased stress [23].

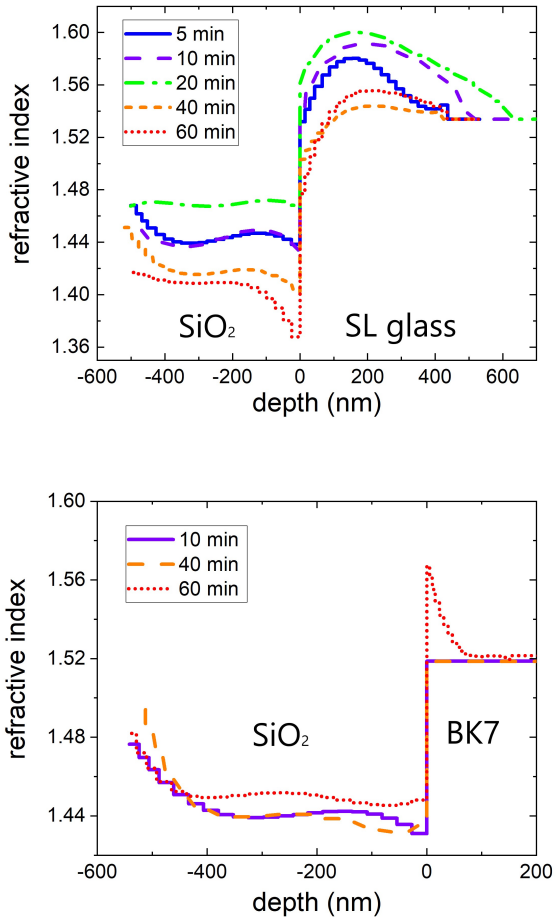

Figure 6: Refractive index profiles ($\lambda = 500$ nm) for different treatment times (top: SL, bottom: BK7 samples) obtained from ellipsometric data fitting. Glass-SiO_2 layer interface is taken at depth equal to 0 nm.

The refractive index profiles for BK7 samples qualitatively presents a similar trend but suggest a much slower dissolution process: only the sample treated for 1 hour shows a refractive index increase at the glass region next to the layer. Compositional characterization revealed a comparable amount of Na^+ in both type substrates (9.3 at.% in SL for 7.6 at.% in BK7). In addition to Na^+, both glasses contain other

alkali ions. We have checked that the presence of other ionic species in the glass does not significantly modify the simulated dynamics, provided that they have a much lower mobility than Na^+. Glass poling studies have reported that Na^+ mobility in BK7 at 300 °C is comparable to the one in SL glass at 200 °C [30]. Therefore, at the same temperature, ion mobility in BK7 glass is expected to be significantly lower than in SL, which can explain the observed slower dynamics. The difference in alkali ion mobilty can also explain that the refractive index peak in glass takes place near the surface in BK7 and at a deeper position in SL substrates. In the case of low alkali ion mobility the glass region next to the layer is weakly depleted of ions and the refractive index profile in the glass is primarily determined by the dopant ion distribution, that peaks in the glass region next to the layer. Under the same treatment conditions, if the alkali ion mobility is large the glass region next to the layer becomes strongly ion-depleted. Then the refractive index maximum in the glass will be determined by the balance between alkali ions decrease and dopant ion increase and may take place away from the surface in contact with the layer.

SIMS measurements were carried out on selected samples to test the insights from numerical modelling and ellipsometric data analysis (Figure 7). The measurements verify the presence of dopant ions in the SiO_2 layer, preferentially in the region next to the side that was facing the anode, and also at the glass region next to the layer. SIMS measurements made on SL samples treated for 20 and 40 minutes indicate that the ratio of Ag concentration peak in the glass and in the layer increases with treatment time. BK7 sample shows a significantly larger amount of Ag in the SiO_2 layer than in the substrate, confirming that the doping process is less advanced than in the SL sample treated for the same time. Finally it has to be pointed out that SIMS measurements show a broad peak in the middle of the layer, that is not predicted by the model but is noticeable in the refractive index profile obtained by

ellipsometry. A possible explanation for this Ag concentration peak could be the presence of hydrogen species during the dissolution process, as reported in [24], and will be the topic of further study. A deeper comparison between ellipsometric and SIMS results regarding the precise extension of Ag distribution in glass is limited by SIMS depth-resolution and the fact that, depending on treatment conditions, samples may show inhomogeneous etching rates during SIMS measurements [31].

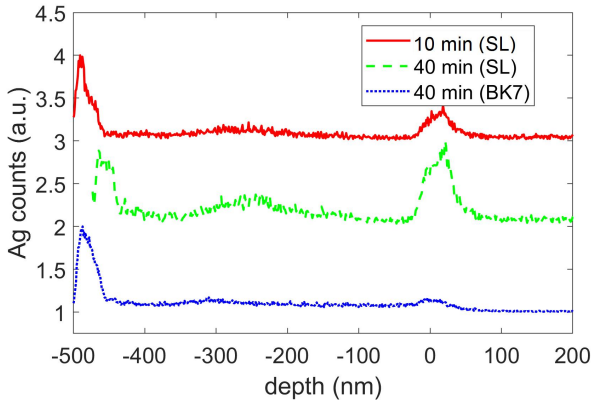

Figure 7: SIMS Ag counts for samples subjected to different EFAD treatment times on SL and BK7 samples.

5. Conclusions

The process of metal doping in dielectric layers on glass substrates has been numerically and experimentally investigated. A model accounting for the drift and diffusion of ions in a dielectric layer/glass system subjected to the application of a DC voltage and elevated temperature enables understanding of the process dynamics. Dopant ion implantation is essentially regulated by the intense electric field generated in the dielectric layer as a result of glass poling. The model elucidates how alkali and dopant ion mobility and alkali concentration affect the distribution of dopant ions in the dielectric layer and glass. The extension of the model to multiple ion species or

time-dependent temperature and voltage is straightforward. Electric field assisted dissolution of Ag films deposited on top of SiO_2/glass systems has been carried out to experimentally study the metal doping process. The high sensitivity of ellipsometric measurements to refractive index in-depth variations allows retrieving information on the dopant ion distribution. The results confirm the trends predicted by the model, such as the concentration of ions in the near-surface layer and glass regions and the progressive redistribution of ions in glass as the process takes place. These trends are further confirmed by SIMS measurements. The results also suggest some unpredicted deviations, like lowering of the SiO_2 layer refractive index for long treatment times, that might be used for building up more advanced models. In summary, this work shows how dielectric thin layer doping by means of electric field assisted metal fiilm dissolution can be controlled by material and process parameters in order to tune dielectric layer optical and compositional properties.

Acknowledgements

This work was financed by Croatian Science Foundation under the project no. IP-2016-06-2168.

References

[1] F. Gonella, Silver doping of glasses, Ceramics International 41 (5) (2015) 6693–6701.

[2] P. Mazzold, S. Carturan, A. Quaranta, C. Sada, V. Sglavo, Ion exchange process: History, evolution and applications, La Rivista del Nuovo Cimento 36 (2013) 397–460.

[3] G. Chartier, P. Collier, A. Guez, P. Jaussaud, Y. Won, Graded-index surface or buried waveguides by ion exchange in glass, Applied Optics 19 (7) (1980) 1092–1095.

[4] F. Gonella, E. Cattaruzza, A. Quaranta, S. Ali, N. Argiolas, C. Sada, Diffusion behavior of transition metals in field-assisted ion-exchanged glasses, Solid State Ionics 177 (35-36) (2006) 3151–3155.

[5] D. Kapila, J. Plawsky, Diffusion processes for integrated waveguide fabrication in glasses: a solid-state electrochemical approach, Chemical Engineering Science 50 (16) (1995) 2589–2600.

[6] A. Lipovskii, V. Melehin, M. Petrov, Y. P. Svirko, V. Zhurikhina, Bleaching versus poling: Comparison of electric field induced phenomena in glasses and glass-metal nanocomposites, Journal of Applied Physics 109 (1) (2011) 1.

[7] F. P. Mezzapesa, I. C. Carvalho, P. G. Kazansky, O. Deparis, M. Kawazu, K. Sakaguchi, Bleaching of sol-gel glass film with embedded gold nanoparticles by thermal poling, Applied Physics Letters 89 (18) (2006) 183121.

[8] J. Sancho-Parramon, V. Janicki, J. Arbiol, H. Zorc, F. Peiro, Electric field assisted dissolution of metal clusters in metal island films for photonic heterostructures, Applied Physics Letters 92 (16) (2008) 163108.

[9] B. Okorn, J. Sancho-Parramon, P. Pervan, I. Fabijanić, V. Janicki, Evolution of electric field assisted dissolution of nanoparticles investigated by spectroscopic ellipsometry, Optical Materials 101 (2020) 109752.

[10] V. Janicki, J. Sancho-Parramon, F. Peiró, J. Arbiol, Three-dimensional photonic microstructures produced by electric field assisted dissolution of metal nanoclusters in multilayer stacks, Applied Physics B 98 (1) (2010) 93.

[11] T. C. Kaspar, J. T. Reiser, J. V. Ryan, N. A. Wall, Nondestructive characterization of corroded glass surfaces by spectroscopic ellipsometry, Journal of Non-Crystalline Solids 481 (2018) 260–266.

[12] I. Fabijanić, P. Pervan, B. Okorn, J. Sancho-Parramon, V. Janicki, Ellipsometry-based study of glass refractive index depth profiles obtained by applying different poling conditions, Applied Optics 59 (5) (2020) A69–A74.

[13] A. Cooper Jr, Electric field buildup and relaxation for chemical diffusion, Journal of Non-Crystalline Solids 14 (1) (1974) 65–78.

[14] S. Batchelor, R. Oven, D. Ashworth, Characterisation of electric field assisted diffused potassium ion planar optical waveguides, Electronics Letters 32 (22) (1996) 2082–2083.

[15] N. Godbout, S. Lacroix, Characterization of thermal poling in silica glasses by current measurements, Journal of Non-Crystalline Solids 316 (2-3) (2003) 338–348.

[16] R. Oven, Modeling the sequential electric field assisted diffusion into glass of two ion species, Journal of Applied Physics 101 (11) (2007) 113113.

[17] M. Petrov, A. Omelchenko, A. Lipovskii, Electric field and spatial charge formation in glasses and glassy nanocomposites, Journal of Applied Physics 109 (9) (2011) 094108.

[18] A. Kudlinski, Y. Quiquempois, G. Martinelli, Modeling of the χ (2) susceptibility time-evolution in thermally poled fused silica, Optics Express 13 (20) (2005) 8015–8024.

[19] M. Petrov, Y. A. Lepen'kin, A. Lipovskii, Polarization of glass containing fast and slow ions, Journal of Applied Physics 112 (4) (2012) 043101.

[20] J. R. Dormand, P. J. Prince, A family of embedded Runge-Kutta formulae, Journal of Computational and Applied Mathematics 6 (1) (1980) 19–26.

[21] T. G. Alley, S. Brueck, R. A. Myers, Space charge dynamics in thermally poled fused silica, Journal of Non-Crystalline Solids 242 (2-3) (1998) 165–176.

[22] A. Von Hippel, E. Gross, J. Jelatis, M. Geller, Photocurrent, space-charge buildup, and field emission in alkali halide crystals, Physical Review 91 (3) (1953) 568.

[23] N. Takamure, A. Kondyurin, D. R. McKenzie, Electric field assisted ion exchange of silver in soda-lime glass: a study of ion depletion layers and interactions with potassium, Journal of Applied Physics 125 (17) (2019) 175104.

[24] E. Borsella, G. De Marchi, F. Caccavale, F. Gonella, G. Mattei, P. Mazzoldi, G. Battaglin, A. Quaranta, A. Miotello, Silver cluster formation in ion-exchanged waveguides: processing technique and phenomenological model, Journal of Non-Crystalline Solids 253 (1-3) (1999) 261–267.

[25] A. N. Miliou, R. Srivastava, R. V. Ramaswamy, Modeling of the index change in K^+–Na^+ ion-exchanged glass, Applied Optics 30 (6) (1991) 674–681.

[26] M. L. Huggins, The refractive index of silicate glasses as a function of composition, Journal of the Optical Society of America 30 (10) (1940) 495–504.

[27] B. Pantchev, Z. Nikolov, Characterization of refractive index profiles in silver-sodium ion-exchanged glass waveguides for homogeneous refracting waveguide structures, IEEE Journal of Quantum Electronics 29 (9) (1993) 2459–2465.

[28] B. Stepanov, J. Ren, T. Wagner, J. Lorincik, M. Frumar, M. Churbanov, Y. Chigirinsky, Solid state field-assisted diffusion of silver in multi-component tellurite glasses, Journal of Non-Crystalline Solids 357 (15) (2011) 3022–3026.

[29] V. Janicki, J. Sancho-Parramon, S. Yulin, M. Flemming, A. Chuvilin, Optical and structural properties of nb2o5–sio2 mixtures in thin films, Surface and Coatings Technology 206 (17) (2012) 3650–3657.

[30] A. L. Brennand, P. G. Kazansky, J. S. Wilkinson, Evaluation of alkali-rich glasses for poling, in: Summaries of Papers Presented at the Lasers and Electro-Optics. CLEO'02. Technical Diges, IEEE, 2002, pp. 236–237.

[31] V. Kaasik, A. Lipovskii, D. Raskhodchikov, I. Reshetov, D. Tagantsev, How to reveal the correct elemental concentration profiles in poled multicomponent silicate glasses from the data of secondary ion mass spectrometry (sims), Journal of Non-Crystalline Solids 503 (2019) 397–399.